Initializing anisotropic electron velocity distribution functions in optical-field ionized plasmas

C-K Huang⬚, C-J Zhang⬚, K A Marsh, C E Clayton and C Joshi

University of California Los Angeles Department of Electrical and Computer Engineering, Los Angeles, CA 90095, United States of America

E-mail: ckhuang@ucla.edu

Abstract

Optical-field ionization (OFI) is often used to produce plasmas for myriad laboratory applications. OFI of gases is known to generate electrons that have anisotropic distributions. In this paper we show that at the time of plasma formation the electron velocity distribution functions can be controlled by changing the wavelength and polarization of the pump laser and ionization state of the plasma. Thomson scattering is used to measure the distinct electron velocity distributions of helium plasmas produced by linearly and circularly polarized laser pulses within a few inverse plasma periods after the plasma formation. In both cases, non-thermal and highly anisotropic initial electron distributions are observed that are consistent with expectations from OFI of both He electrons.

Keywords: optical-field ionization, Thomson scattering, plasma diagnostics, anisotropic distribution function

(Some figures may appear in colour only in the online journal)

1. Introduction

With the advent of ultra-short pulse lasers, optical-field ionized (OFI) dense plasmas are readily generated in the laboratory. The knowledge of the initial velocity distribution of electrons is important for understanding the evolution of such plasmas. Velocity map imaging [1] has been used to directly map the momentum distribution of emitted photo-electrons or ions but this technique is limited to extremely low densities where collisional and collisionless interaction between electrons is negligible. However, for relatively dense OFI plasmas ($n_e > 10^{17} \, \text{cm}^{-3}$), there is surprisingly a lack of comprehensive measurements of their initial electron velocity distribution functions (EVDF). In this paper, we show that by changing polarization, wavelength of the ionizing laser and the ionization state of the plasma, the initial EVDF of an OFI plasma can be manipulated. These distributions are generally non-thermal and highly anisotropic. Kinetic theory predicts that such plasmas are unstable to kinetic instabilities [2–6]. OFI plasmas are relevant to plasma-based acceleration [7],

plasma channel formation [8, 9] and recombination x-ray lasers [10]. For instance, in experiments that use PW-class laser pulses, the prepulse could easily produce a plasma with a distribution function that is susceptible to rapidly developing magnetic fields induced by kinetic instabilities [11]. In this paper we experimentally demonstrate two examples of nonthermal and anisotropic distribution functions by ionizing both electrons of He using fs-class linearly and circularly polarized laser pulses.

Optical-field ionization of gases becomes dominant over multi-photon ionization when the Keldysh parameter is in the tunnel ionization regime, i.e. $\gamma = (U_i/2U_p)^{1/2} \ll 1$ where U_i is the ionization potential and U_p is the ponderomotive potential of the laser [12]. The energy and the direction of the ionized electron in OFI depends upon the details of the laser pulse(s) and the ionization state of the gas [13–16]. The electrons are ejected transverse to the wave vector of the laser pulse along the direction of its polarization in the non-relativistic limit ($a_0 \leqslant 1$), producing strongly non-thermal and/or anisotropic EVDF in the resulting plasma. Here $a_0 = eA/mc^2 = eE/m\omega c$

is the normalized laser strength parameter, where A is the magnetic vector potential, E is the laser electric field, and ω is the laser frequency. The EVDF of highly charged states produced by relativistic pulses ($a_0 \geqslant 1$) in a dense plasma are rather complicated because they can be affected by numerous other physical effects such as wakefields/parametric instabilities [7, 17], direct energy exchange with the laser field [18] and therefore will not be considered here. The polarization dependence of OFI produced electrons has been tested in previous work in either the long-wavelength [13] or the barrier suppression limit using very low-pressure gases [19, 20]. Leemans *et al* [21] showed that it was possible to control the Raman instability by varying the polarization of a 200 ps CO_2 laser produced OFI plasma. Moore *et al* [22] showed that when intense ($a_0 \sim O(1)$), longer laser pulses are used, the electrons gain additional energy from the ponderomotive potential of the laser envelope. Glover *et al* [23] used Thomson scattering diagnostic to fit the scattered light spectrum from an OFI He plasma produced using a linearly polarized 800 nm pulse but they did not observe scattering from each of the two ionic species of He. Thus, no experimental confirmation of the nonthermal and/or highly anisotropic initial EVDF characteristic of OFI plasmas has been made to-date even though the kinetic instabilities that follow the creation of such plasmas have been predicted [3–5].

2. Simulations of initial distribution functions

In figure 1 we show four examples of such EVDF in velocity space (v_x versus v_y) using the 3D particle-in-cell code OSIRIS [24] where the formation of a fully ionized, dense ($5 \times 10^{18} \, \text{cm}^{-3}$) He plasma is modeled using the ADK theory [25]. The dimensions of the simulation box are $63.6 \times 35.6 \times 35.6 \, \mu\text{m}$ in the z, x and y directions. In all cases the simulations consider tunnel ionization of electrons [12] ($\gamma_{\text{He}^{1+}} = 0.38$ and $\gamma_{\text{He}^{2+}} = 0.23$) and self-consistently include other physical effects such as the ponderomotive force of the optical pulse, plasma kinetic effects, and wake formation. We shall refer to the electron that ionizes first as the He^{1+} electron and second as the He^{2+} electron. Here the x–y plane is perpendicular to the direction of propagation of the laser, z. The electrons used to generate the EVDF shown in figure 1 are those within a $\Delta z = 2 \, \mu\text{m}$ slab right after the laser pulse. In these cases the He^{1+} electrons are ionized early during the risetime of the laser pulse within a few laser cycles and the He^{2+} electrons are ionized approximately 10 fs after the first He electron. These electrons have both transverse (x and y) and longitudinal (z) oscillating energy of a few eV due to a weak linear wake formed by the laser pulse [7] and the ions are essentially cold in all directions.

We manipulate the EVDF in figure 1 by changing the polarization of the laser pulse to ionize He atoms from linear (a), to elliptical (b) to circular (c), (d). Figure 1(a) shows that the initial electron distribution along the laser polarization direction (y) in the linear polarization (LP) case can be well described by a sum of two 1D (near) Maxwellian distributions with
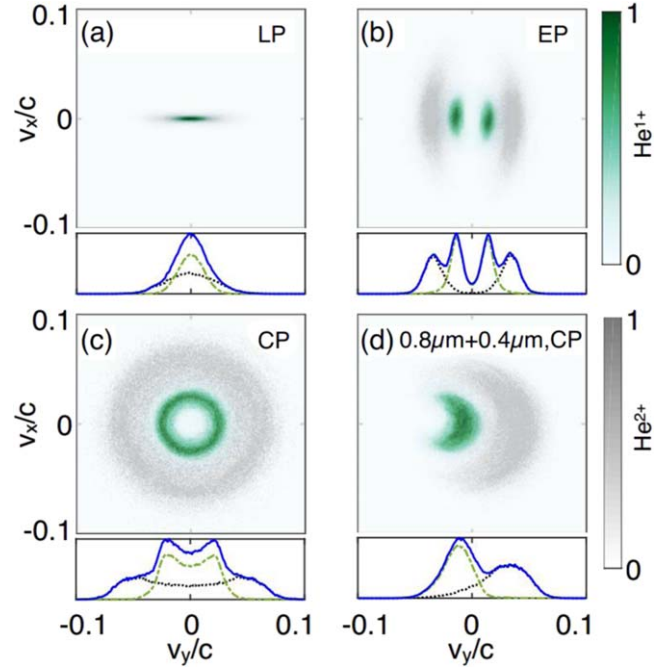
Figure 1. (a)–(c) Examples of simulated electron velocity distributions using OSIRIS of He plasmas produced by 50 fs, 800 nm laser pulses with peak intensity of $1.6 \times 10^{17} \, \text{W cm}^{-2}$ and different polarizations (linear, elliptical, circular respectively). (d) Circular, 800 nm, $3 \times 10^{16} \, \text{W cm}^{-2}$ + circular, 400 nm, $1 \times 10^{16} \, \text{W cm}^{-2}$ with the same initial phase. Also shown below each v_x–v_y image is the v_y distribution (the sum of the number of particles at each v_y) for He^{1+} electrons (dashed green curve), He^{2+} electrons (dotted black curve) and their sum (solid blue line).

temperatures of 60 eV (He^{1+}) and 210 eV (He^{2+}) respectively. In the elliptical polarization case (degree of ellipticity $\alpha = 0.5$, (figure 1(b)) the EVDF shows four lobes with the distribution in x much wider than that in y. Once again the He^{2+} electrons (gray) are more energetic than He^{1+} electrons. In the circular polarization (CP) case (figure 1(c)), electron distributions are donut-shaped in the x–y velocity space. The distributions of He^{1+} and He^{2+} electrons correspond to the inner and the outer ring of the distribution in figure 1(c). Although this specific type of EVDF has not been treated in rigorous theoretical analysis, a single ring distribution has been studied analytically using kinetic theory and it is shown to be susceptible to developing kinetic instabilities [5, 6, 26]. The existence of electrons close to zero transverse velocity suggests that the plasma has already evolved by the end of the laser pulse, due to collective effects. The overall initial electron distribution in the circular case is also shown in figure 1(c), blue curve. It indicates a highly non-Maxwellian distribution with much hotter root mean square (rms) temperature of $\sim 470 \, \text{eV}$ (220 eV and 910 eV for the He^{1+} and the He^{2+} electrons respectively). In case 1(d) a two frequency CP laser pulse with different intensities generates a bump-on-tail distribution that would lead to spontaneous generation of plasma waves via inverse Landau damping. From the above examples, it is clear that numerous other 'designer' EVDF are possible by optimization of laser and choice of the ionizing medium.
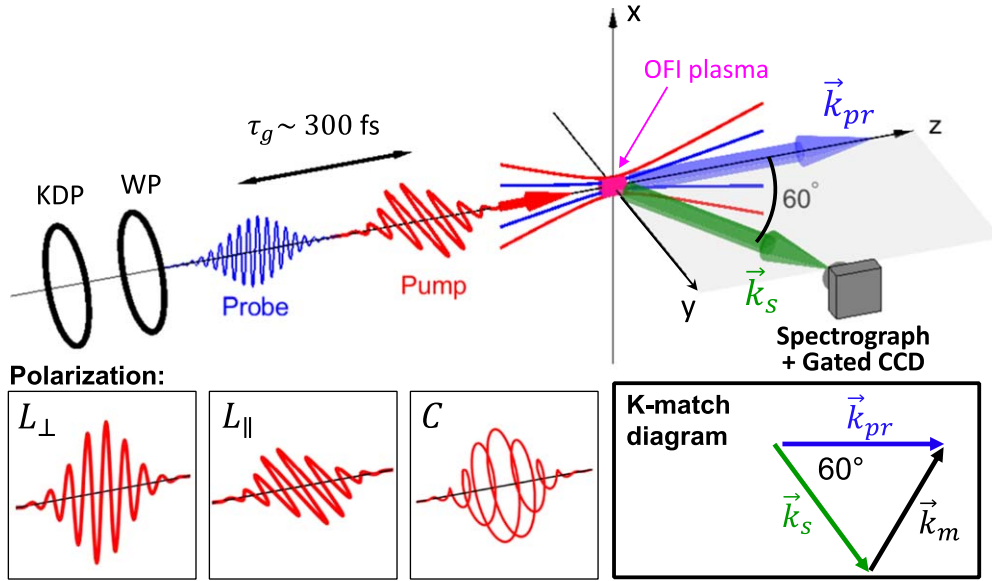
Figure 2. Schematic of the experiment. The 800 nm pump beam generates OFI plasmas that are probed by a collinear 400 nm Thomson scattering beam using a fixed delay: linear polarization perpendicular to the scattering plane ($L_\perp$), parallel to the scattering plane ($L_\parallel$) and circular polarization (C). Also shown is the *k*-matching diagram where the vector $\vec{k}_m$ is probed in Thomson scattering. KDP: KDP crystal; WP: half-wave plate for linear polarization or quarter-wave plate for CP.
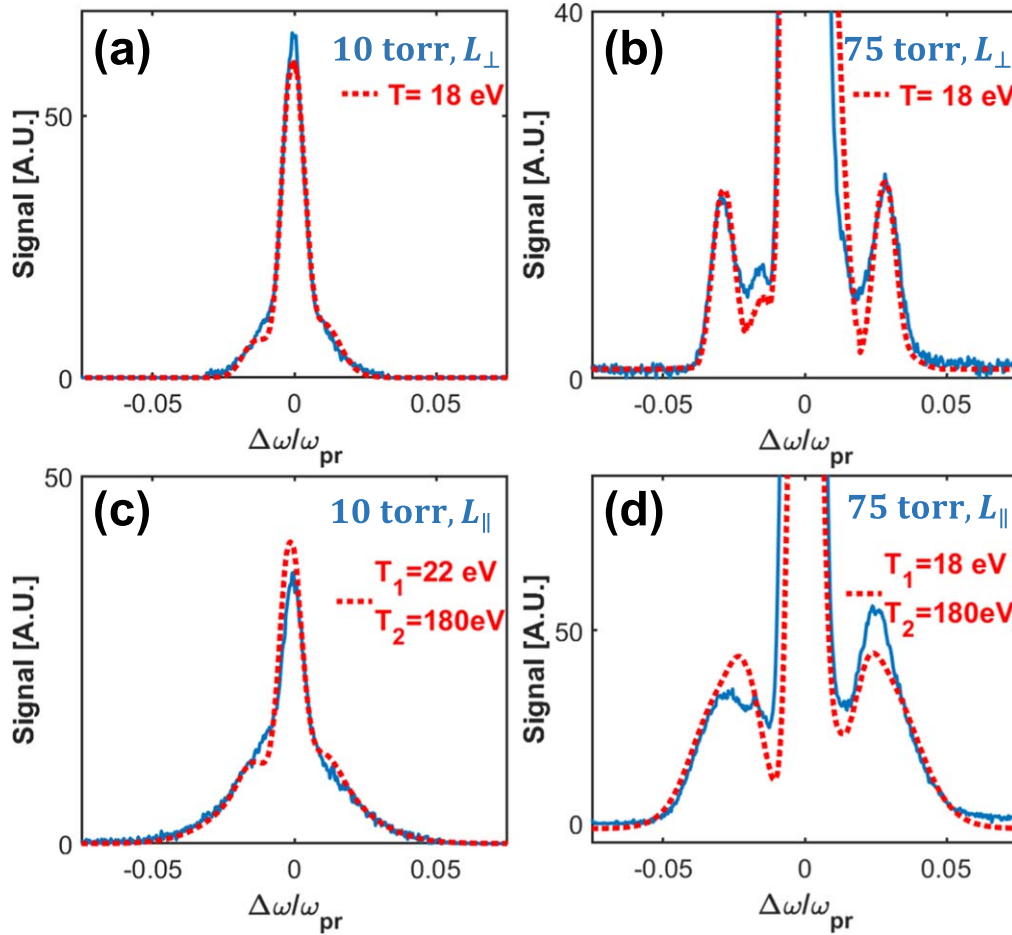
3. Experiments

As mentioned earlier, the measurement of the EVDF is difficult because plasmas begin to isotropize very quickly because of kinetic instabilities. These collisionless processes tend to isotropize the initially produced EVDF on a timescale far shorter than electron–electron or electron–ion collisions alone, estimated to be tens of ps for typical value of $T_{x,y}/T_z$ expected here. We therefore use the Thomson scattering diagnostic with ∼90 fs (FWHM) probe pulses to interrogate the EVDF of the OFI helium plasma just ∼300 fs after ionization is completed. During such a short time period plasma density evolution due to expansion or recombination can be neglected.

3.1. Experimental setup

The experimental setup is shown schematically in figure 2. The plasma was formed by ionizing a static fill of He gas at various pressures by focusing a 800 nm, ∼50 fs (FWHM) duration laser pulse containing ∼10 mJ energy. The laser was focused by an off-axis parabolic mirror (OAP) to a spot size $2w_0$ of 16 μm giving a peak intensity of ∼1 × 10^{17} W cm^{-2}. The ∼1 mJ, ∼90 fs (FWHM), 400 nm probe pulse is generated by a 1.5 mm thick KDP crystal. The probe beam was focused by the same OAP and focused to a even smaller spot size within the fully ionized plasma. Thomson scattered light was collected at 60° with respect to (w.r.t.) the incident pulse by a one-to-one imaging system that relays image of the central part of the plasma to the entrance slit of the spectrograph. The spectrometer consists of a Czerny–Turner spectrograph (ISA HR320) coupled with a time-gated intensified CCD (Princeton Instrument PI-MAX4). The gate width

and the gate delay of the intensified CCD were set to optimize the Thomson scattered signal and minimize the stray light from plasma recombination emission and from other objects inside the chamber. The experimental spectra were corrected for the spectral transmission of the system as well as subtracting the stray light from the vacuum chamber. The effects of the second harmonic generation, the dispersion and the group delay between the pump and the probe pulses were calculated using a simulation software SNLO. The simulation shows there is nearly no change of the pulse shape for the pump beam in the case of a 12 mJ, 50 fs (FWHM), 800 nm input. The group delay between the 800 nm pump beam and the 400 nm probe beam is estimated to be 300 fs.

The plane containing the incident probe wave vector ($\vec{k}_{pr}$) and the scattered light wave vector ($\vec{k}_s$) is referred to as the scattering plane. Two polarization configurations for linearly (L) polarized pump beams are the polarization direction parallel ($L_\parallel$) or perpendicular ($L_\perp$) to the scattering plane. The $L_\parallel(L_\perp)$ polarization allows us to independently probe the EVDF essentially along the v_y (v_x) directions as shown in figure 1(a). There is only one configuration for CP (C) since the 'double donut' EVDF generated is transversely isotropic (figure 1(c)). The control of polarization was achieved by inserting waveplates (half-wave plate for LP and quarter-wave plate for CP) between the KDP crystal and the OAP. The half-wave plate which is designed for 800 nm light has no effect on the polarization of the 400 nm probe beam, but the quarter waveplate will rotate the probe beam polarization by 90° (parallel to the scattering plane). While the polarization of the probe pulse has no influence on the spectral shapes, it affects the scattered power collected in the experiment, and the signal strength for CP is reduced by a factor of 2.

Figure 3. Thomson scattering spectra for linear polarization (blue curves—experimental spectra; dotted red curves—calculated spectra). Polarization direction is out of the scattering plane for (a) and (b) and parallel to the scattering plane for (c) and (d). The $L_\perp$ cases can be fit by a single temperature of 18 eV whereas the $L_\parallel$ cases require a two-temperature fit as shown.
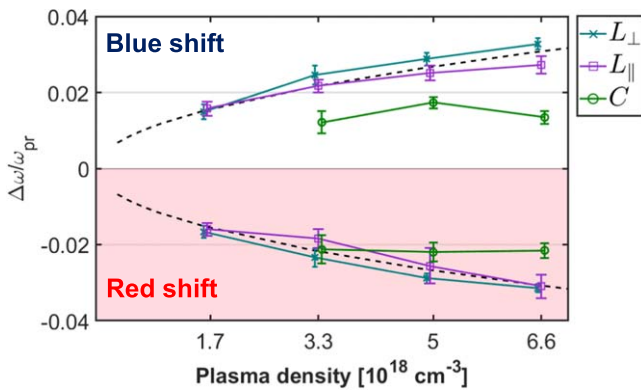
Figure 4. The measured spectral peak shifts of the electron feature for different plasma densities and different laser polarization ($L_\perp$, $L_\parallel$, C). The error bars show the standard deviation of the shifts for 100 shots. The plasma densities plotted correspond to fully ionized He at 25, 50, 75, and 100 Torr. The dashed lines show the variation of frequency shift equal to the plasma frequency, $\Delta\omega = \omega_{pe}(n_e)$.

3.2. Spectral fittings

The measured scattered spectra are used to infer the near instantaneous status of OFI plasmas by comparing them with the Thomson scattering theory [27]. All the data shown in this

paper are the average of 200 consecutive shots to improve the signal-to-noise ratio. For a non-relativistic, non-magnetized plasma with an electron distribution function $f_e(\vec{v})$ and an ion distribution function $f_i(\vec{v})$, Thomson scattering spectral power density (SPD) function can be written as

$$S(\vec{k}, \omega) = \frac{2\pi}{k} \left| 1 - \frac{\chi_e}{\epsilon} \right|^2 f_e\left(\frac{\omega}{k}\right)$$
$$+ \frac{2\pi Z}{k} \left| \frac{\chi_e}{\epsilon} \right|^2 f_i\left(\frac{\omega}{k}\right), \tag{1}$$

where Z is the atomic number of the atom, $\epsilon = 1 + \chi_e + \chi_i$ is the dielectric function, χ_e and χ_i are the electron and ion susceptibilities. We can apply arbitrary distribution functions f_e and f_i to calculate $S(\vec{k}, \omega)$ and get the spectral shape of the Thomson scattered light. Due to the broad bandwidth of the probe beam ($\sim$3.4 nm) and the limiting wavelength resolution ($\sim$1 nm) of the spectrograph, the ion feature spectrum is not resolved in our experiment and thus information about the plasma comes from the first term in equation (1) convolved with both spectral distribution of the probe beam and instrument function of the spectrograph. The 60° scattering angle determines the measured $\vec{k}_m$ in this experiment as depicted in figure 2. It should be noted that the temperatures
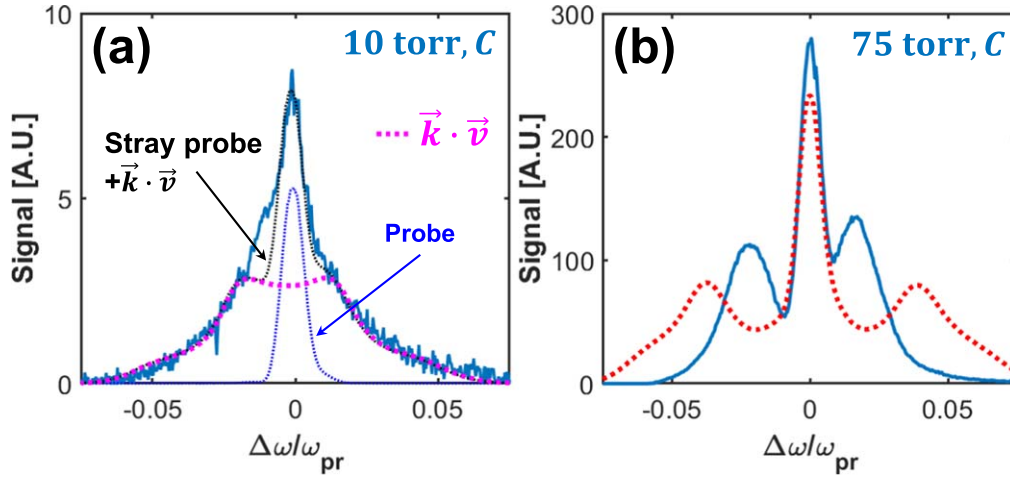
Figure 5. Thomson scattering spectra for circular polarization averaged over 200 shots: (a) the measured spectrum at 10 Torr He pressure and a fit that is the sum of the Doppler shifted spectrum (dotted pink curve) expected from the electron distribution shown in figure 1(c) and stray light spectrum of the probe beam (dotted blue curve). (b) The measured Thomson scattered spectrum at 75 Torr (blue curve) and the calculated spectrum (dotted red curve) using a distribution with two pairs of drifting Maxwellian counter streams (drift velocities of $\pm0.015c$ and $\pm0.046c$, widths of 87 and 79 eV, and a density ratio of ∼4:1) deduced from the EVDF shown in figure 1(c).

of the two-Maxwellian distributions in the experiments are expected to be different than those from the simulations since we observe the plasma along $\vec{k_m}$ which has a $30°$ angle with respect to the transverse plane used in simulations. The observable temperatures, which are evaluated from the projection of the distribution onto the measured wavevector [28], are about 45 and 160 eV for polarization $L_\parallel$.

4. Results and discussion

The scattered light spectra from plasmas produced by LP pump taken at two fill pressures are shown in figure 3. The central spectral feature at around 400 nm is the ion feature which is not frequency resolved in this experiment. The frequency shift of the 'electron feature', which is associated with collective scattering from electron plasma waves is symmetric on either side of the ion feature. The red dashed line in each plot is the best fit of the calculated SPD function $S(\omega)$. Figures 3(a) and (b) show the spectra where the polarization is perpendicular to the scattering plane ($L_\perp$). We found that a single Maxwellian distribution with electron temperature of 18 ± 2 eV (room temperature ions) fits spectra obtained at both low (10 Torr) and high (75 Torr) pressures. The corresponding temperature in the perpendicular plane after 300 fs is expected to be ∼12 eV from simulations. Thus there is a reasonable agreement between the experiment and the simulations.

The scattering spectra when the LP is in the scattering plane $L_\parallel$ are shown in figures 3(c) and (d) also for helium fill pressures of 10 and 75 Torr respectively. In this case, the calculated SPD functions given by a single Maxwellian distribution (not shown) do not fit with the experimental spectra. The data were therefore fitted by taking a two-temperature distribution into consideration. Substituting $f_e = 0.5f_{e,T_1} + 0.5f_{e,T_2}$ into equation (1) where T_1 and T_2 are fitting parameters ($T_2 > T_1$) while keeping the ions as a fixed ultra-cold component, we get a new set of

SPD functions that describe the scattering spectra for the LP case. The best fits give $T_1 = 20 \pm 2$ eV and $T_2 = 180 \pm 20$ eV. The agreement here with the simulations is again reasonable. We can see that the theoretical plots shown figures 3(c) and (d) fit less well than those for figures 3(a) and (b) both taken at the same pressure but in the orthogonal plane.

The frequency shift of the electron feature in the collective scattering regime should increase as the Langmuir wave frequency, ω_{pe}. Figure 4 shows the measured spectral peak shifts for various plasma densities for different polarization configurations. For both $L_\perp$ and $L_\parallel$, the shifts of their sideband peaks both increase with densities as expected. This is clearly not the case for CP case which is also shown. The frequency shift of the electron feature for the CP case was almost independent of the plasma density, which is indicative of some other collective phenomena that are relatively insensitive to the plasma density in this range being the dominant collective scattering mechanism than the usual Langmuir waves.

The Thomson scattered spectra for the CP pump pulses are shown in figure 5. Recall that the electrons in this case have higher average kinetic energy than those with LP and the EVDF deviate greatly from Maxwellian. Our fitting attempt using equation (1) failed with either one-temperature or two-temperature Maxwellian distributions as expected. At low enough plasma densities collective effects are not important and one expects photons to be Doppler up or down shifted because of the individual electron motion. We found that it is possible to fit the experimental spectrum taken at this low plasma density using the distribution function observed in the simulation (without any assumption made about rms temperature) as shown in figure 1(c). The calculated SPD fits to the wings of the total measured spectrum at a plasma density of 6.6×10^{17} cm^{-3} used in the experiment. When the spectrum of the stray probe photons is also taken into account the overall Doppler shifted plus the stray photon spectrum fits the experimentally measured spectrum extremely well. This

excellent fit between the experimental scattered light spectrum and the calculated Doppler shifted photon spectrum shows that the EVDF shown in figure 1(c) for the CP case exists in the plasma. For the higher density case (figure 5(b)) two distinct spectral 'electron' peaks with asymmetric shifts appeared. Their frequency shifts were both $\leqslant \omega_{pe}$ and independent of the plasma density in contrast with the case of LP shown in figure 4. This is expected if the scattering is from the density fluctuation induced by the electron plasma waves whose frequency are lower than the plasma frequency. Time-resolved measurement has confirmed and quantified the growth of the unstable modes in OFI helium plasmas produced by both CP and LP laser pulses [29]. The result shows that a high-frequency mode grows and damps within 1 ps in the CP case and it takes more than 1 ps for the similar mode to grow in the LP case.

5. Conclusion

In conclusion, we have demonstrated that OFI is a method for controlling the initial EVDF in plasmas. We have used Thomson scattering diagnostic to probe two such EVDF within 300 fs of their initialization by OFI in He plasmas using different polarization configurations. The scattered light spectra are consistent with the expected anisotropic distributions. Until they are isotropized and thermalized such plasmas cannot be described by the fluid theory and thus present a platform for studying kinetic effects and instabilities in laboratory plasmas.

Acknowledgments

ORCID iDs

C-K Huang https://orcid.org/0000-0002-4478-0542
C-J Zhang https://orcid.org/0000-0001-8035-3014

References

[1] Eppink A T J B and Parker D H 1997 Velocity map imaging of ions and electrons using electrostatic lenses: application in photoelectron and photofragment ion imaging of molecular oxygen *Rev. Sci. Instrum* **68** 3477–84

[2] Davidson R C 1983 Kinetic waves and instabilities in a uniform plasma *Handbook of Plasma Physics* ed A A Galeev and R N Sudan vol 1 (Amsterdam: North-Holland) p 229

[3] Krainov V P 2003 Weibel instability in plasma produced by a superintense femtosecond laser pulse *J. Exp. Theor. Phys.* **96** 430–5

[4] Bychenkov V Y, Romanov D V, Rozmus W, Capjack C E and Fedosejevs R 2006 Distinctive features of photoionized plasma from short x-ray-pulse interaction with gaseous medium *Phys. Plasmas* **13** 013101

[5] Vagin K Y and Uryupin S A 2017 Electron modes of plasma generated at tunnel ionization of atoms by a circularly polarized radiation *Phys. Plasmas* **24** 103118

[6] Vagin K Y and Uryupin S A 2016 Amplification of electromagnetic pulses by photoionized plasma *J. Russ. Laser Res.* **37** 473–83

[7] Joshi C 2006 Plasma accelerators *Sci. Am.* **294** 40–7

[8] Lemos N, Cardoso L, Geada J, Figueira G, Albert F and Dias J M 2018 Guiding of laser pulses in plasma waveguides created by linearly-polarized femtosecond laser pulses *Sci. Rep.* **8** 3165

[9] Shalloo R J, Arran C *et al* 2019 Low-density hydrodynamic optical-field-ionized plasma channels generated with an axicon lens *Phys. Rev. Accel. Beams* **22** 041302

[10] Burnett N H and Corkum P B 1989 Cold-plasma production for recombination extreme-ultraviolet lasers by optical-field-induced ionization *J. Opt. Soc. Am.* B **6** 1195–9

[11] Romanov D V, Bychenkov V Y, Rozmus W, Capjack C E and Fedosejevs R 2004 Self-organization of a plasma due to 3d evolution of the weibel instability *Phys. Rev. Lett.* **93** 215004

[12] Keldysh L V 1965 Ionization in the field of a strong electromagnetic wave *Sov. Phys. JETP* **20** 1307

[13] Corkum P B, Burnett N H and Brunel F 1989 Above-threshold ionization in the long-wavelength limit *Phys. Rev. Lett.* **62** 1259–62

[14] Zhang L *et al* 2014 Laser-sub-cycle two-dimensional electron-momentum mapping using orthogonal two-color fields *Phys. Rev.* A **90** 061401

[15] Dimitrovski D, Maurer J, Stapelfeldt H and Madsen L B 2014 Low-energy photoelectrons in strong-field ionization by laser pulses with large ellipticity *Phys. Rev. Lett.* **113** 103005

[16] Mancuso C A *et al* 2015 Strong-field ionization with two-color circularly polarized laser fields *Phys. Rev.* A **91** 031402

[17] Joshi C, Tajima T, Dawson J M, Baldis H A and Ebrahim N A 1981 Forward raman instability and electron acceleration *Phys. Rev. Lett.* **47** 1285–8

[18] Shaw J L, Lemos N, Amorim L D, Vafaei-Najafabadi N, Marsh K A, Tsung F S, Mori W B and Joshi C 2017 Role of direct laser acceleration of electrons in a laser wakefield accelerator with ionization injection *Phys. Rev. Lett.* **118** 064801

[19] Mohideen U, Sher M H, Tom H W K, Aumiller G D, Wood O R, Freeman R R, Bokor J and Bucksbaum P H 1993 High intensity above-threshold ionization of he *Phys. Rev. Lett.* **71** 509–12

[20] McNaught S J, Knauer J P and Meyerhofer D D 1997 Measurement of the initial condition of electrons ionized by a linearly polarized, high-intensity laser *Phys. Rev. Lett.* **78** 626–9

[21] Leemans W P, Clayton C E, Mori W B, Marsh K A, Dyson A and Joshi C 1992 Plasma physics aspects of tunnel-ionized gases *Phys. Rev. Lett.* **68** 321–4

[22] Moore C I, Ting A, McNaught S J, Qiu J, Burris H R and Sprangle P 1999 A laser-accelerator injector based on laser ionization and ponderomotive acceleration of electrons *Phys. Rev. Lett.* **82** 1688–91

[23] Glover T E, Donnelly T D, Lipman E A, Sullivan A and Falcone R W 1994 Subpicosecond thomson scattering measurements of optically ionized helium plasmas *Phys. Rev. Lett.* **73** 78–81

[24] Fonseca R A *et al* 2002 Osiris: a three-dimensional, fully relativistic particle in cell code for modeling plasma based accelerators *In Lect. Notes Comput. Sci.* (Berlin: Springer) pp 342–51

[25] Ammosov M V, Delone N B and Krainov V P 1986 Tunnel ionization of complex atoms and of atomic ions in an alternating electromagnetic field *Sov. Phys. JETP* **64** 1191

[26] Peter Yoon H and Ronald C 1987 Davidson. Exact analytical model of the classical weibel instability in a relativistic anisotropic plasma *Phys. Rev.* A **35** 2718–21

[27] Froula D H, Glenzer S H, Luhmann N C and Sheffield J 2011 *Plasma Scattering of Electromagnetic Radiation* 2nd edn (Cambridge: Academic) ch 3 pp 45–68

[28] Chegotov M V 2000 Thomson scattering in a plasma created by a short intense laser pulse *Plasma Phys. Rep.* **26** 602–5

[29] Zhang C, Huang C-K, Marsh K A, Clayton C E, Mori W B and Joshi C 2019 Ultrafast optical field-ionized gases-a laboratory platform for studying kinetic plasma instabilities *Sci. Adv.* **5** 9